Improved Reissner-Nordström-(A)dS Black Hole in Asymptotic Safety

Cristopher González* and Benjamin Koch†

Instituto de Física,

Pontificia Universidad Católica de Chile,

Av. Vicuña Mackenna 4860,

Santiago, Chile

Abstract

This paper studies the quantum modifications of the Reissner-Nordström-(A)dS black hole within Quantum Einstein Gravity, coupled to an electromagnetic sector. Quantum effects are introduced on the level of the improvements of the classical solution, where the originally constant couplings (G_0, Λ_0, and α_0) are promoted to scale dependent quantities (G_k, Λ_k, and α_k). Those running couplings are calculated in the functional renormalization group approach. A crucial point of this, so called "improving solutions" procedure is the scale setting where the arbitrary scale k acquires physical meaning due to a relation to the coordinate scale r. It is proposed to use such scale settings which are stable after iterative improvements. Using this method one finds that for those improved solutions, there is no stable remnant and due to the appearance of a new internal horizon, there is also no necessity to impose a minimal black hole mass for charged black holes, in order to avoid the the cosmic censorship hypothesis.

PACS numbers: 04.20.Dw, 04.62.+v, 04.70.Bw, 04.70.Dy, 11.10.Hi

Keywords: Black Holes; Quantum Gravity; Asymptotic Safety; Renormalization Group

* cdgonzalez1@uc.cl

† bkoch@fis.puc.cl

CONTENTS

I. INTRODUCTION

Classical black holes are classical solutions of the equations of general relativity that have attracted a lot of interest. The Schwarzschild and the Kerr-Newman black holes are excellent candidates for numerous astrophysical observations [1, 2]. Apart from this observational fact, black hole solutions are also theoretically extremely interesting objects [3], since they allow to study the theory of general relativity at its limits of validity: The transition from classical to quantum. The famous Hawking radiation [4, 5] is exemplary for this interplay between classical geometry and quantum physics. An other interesting example are charged Reissner-Nordström black holes, which via the cosmic censorship hypothesis proposed by Roger Penrose [6–9] allows to derive a minimal mass to charge ratio for viable black holes. This hypothesis is an open question in theoretical physics and there is no general proof of its validity, however, there are studies that approve and

disapprove this conjecture in different scenarios [10–12].

It is well known, the formulation of a quantum version of general relativity is facing serious problems and among the approaches that try to address this problem, Weinbergs Asymptotic Safety (AS) scenario is a serious candidate [8, 13]. The key point of this idea is that it conjectures the existence of a non-Gaussian Fixed Point (NGFP) in the flow of the dimensionless couplings of the gravitational theory [14]. With the techniques of the Functional Renormalization Group (FRG) one can derive non-perturbative flow equations which allow to study this idea in practice. Strong evidence for the existence of a non-trivial Ultra Violet (UV) fixed point has been found [15–20]. This, is a very important formal result and the question arises whether and how it is manifest in specific gravitation systems.

Given the importance of black hole physics as testing ground for quantum gravity candidates, it is clear that within AS and FRG one will have to say something about black holes. In order to estimate the leading effects of AS on black holes one can borrow a tool from early quantum electro dynamics. In this very well tested quantum field theory leading quantum corrections to the classical Coulomb potential can be obtained by the "improving solutions" scheme, leading to the Uehling potential [21]. Even though for next to leading results, other techniques turned out to be more precise, the leading effects can still be cast within the "improving solutions" language. This technique can be straight forwardly adapted to classical black hole solutions in general relativity. There exist numerous studies on this subject in terms of using FRG results in order to determine quantum corrections to the classical solution [22–29], most prominently the Schwarzschild, the (Anti)-de Sitter ((A)dS), and the Kerr black hole. This work represents a logical continuation of those studies in the sense that it explores the AS-FRG effects on the Reissner-Nordström (RN) solution (and (A)dS-RN black hole), where particular attention is dedicated to the cosmic censorship.

This paper is organized as follows: In section II the most relevant classical properties of the Reissner-Nordström solution are summarized. In section III the RG flow of Quantum Einstein Gravity (QEG) coupled to Quantum Electrodynamics (QED) is given. Connecting the formal FRG results to physical results in the context of black hole physics involves a scale setting procedure. This is given in section IV. The FRG improvement of the Reissner-Nordström solution, based on this scale setting, is presented in section V. Within this, the improved line element, a new iterative improvement and comparison of alternative improvement schemes, the modified horizon structure, the cosmic censorship, improved temperature and the modified mass and charge of the black hole are discussed. Finally, the results are summarized and commented with concluding remarks in section VI.

II. CLASSICAL RN BLACK HOLES

The classical solution for a charged spherically symmetric black hole with cosmological constant is given by the line element [30–32]

$$ds^2 = -f(r)dt^2 + \frac{dr^2}{f(r)} + r^2 d\Omega^2 \ , \tag{2.1}$$

where

$$f_{cl}(r) = 1 - \frac{2G_0 M_0}{r} + \frac{G_0 Q_0^2}{\alpha_0 r^2} - \frac{1}{3}\Lambda_0 r^2 \ . \tag{2.2}$$

Like in most of the literature the units are chosen such that $c = \hbar = 1$, whereas the electromagnetic fine structure constant $\alpha_0 \equiv \frac{e^2}{4\pi}$ is kept explicit. It is well know this solution collapses for small values of the radial coordinate, which can be seen from evaluating invariant quantities such as the Kretschmann scalar in this limit

$$R_{\mu\nu\rho\sigma}R^{\mu\nu\rho\sigma} = \frac{48G_0^2M_0^2}{r^6} + \frac{56G_0^2Q_0^4}{\alpha_0^2 r^8} - \frac{96G_0^2M_0Q_0^2}{\alpha_0 r^7} + \frac{8}{3}\Lambda_0^2 \ , \tag{2.3}$$

One observes that the first two leading divergencies are dominated by the charge parameter Q_0 and that the subleading $1/r^6$ divergence is the one known from the Schwarzschild solution. The possible horizons are given by the zeros of the function (2.2)

$$r_1 = \quad \rho^{1/2} - \left[\frac{3}{2\Lambda_0} - \rho - \frac{3G_0M_0}{2\Lambda_0}\rho^{-1/2}\right]^{1/2}, \tag{2.4}$$

$$r_2 = \quad \rho^{1/2} + \left[\frac{3}{2\Lambda_0} - \rho - \frac{3G_0M_0}{2\Lambda_0}\rho^{-1/2}\right]^{1/2}, \tag{2.5}$$

$$r_3 = -\rho^{1/2} - \left[\frac{3}{2\Lambda_0} - \rho + \frac{3G_0M_0}{2\Lambda_0}\rho^{-1/2}\right]^{1/2}, \tag{2.6}$$

$$r_4 = -\rho^{1/2} + \left[\frac{3}{2\Lambda_0} - \rho + \frac{3G_0M_0}{2\Lambda_0}\rho^{-1/2}\right]^{1/2}, \tag{2.7}$$

where

$$\rho = \frac{1}{2\Lambda_0}\left[1 - \frac{\mathcal{R}^{-1/3}\mathcal{R}_2}{2\alpha_0} - \frac{\mathcal{R}^{1/3}}{2\alpha_0}\right], \tag{2.8}$$

$$\mathcal{R} = \mathcal{R}_1 + \sqrt{{\mathcal{R}_1}^2 - {\mathcal{R}_2}^3}, \tag{2.9}$$

$$\mathcal{R}_1 = \alpha_0^3 + 12G_0Q_0^2\alpha_0^2\Lambda_0 - 18G_0^2M_0^2\alpha_0^3\Lambda_0, \tag{2.10}$$

$$\mathcal{R}_2 = \alpha_0^2 - 4G_0Q_0^2\alpha_0\Lambda_0. \tag{2.11}$$

Out of those four candidates, only those correspond to physical horizons that are real and positive valued. In order to have at least one physical horizon it is necessary that $\mathcal{R}_1^2 - \mathcal{R}_2^3 \geq 0$ in (2.9). This implies that there exists a minimal value for the mass parameter M_0, associated with a critical black hole with at least one degenerate horizon. This critical value is obtained by writing out the (in)equality explicitly

$$81G_0^3\alpha_0^3\Lambda_0M_0^4 - (9G_0\alpha_0^3 + 108G_0^2Q_0^2\alpha_0^2\Lambda_0)M_0^2 + 24G_0Q_0^4\alpha_0\Lambda_0 + 16G_0^2Q_0^6\Lambda_0^2 + 9Q_0^2\alpha_0^2 = 0,$$

and solving for the mass parameter M_0. The two positive valued solutions are

$$M_1 = \frac{1}{3G_0}\sqrt{\frac{6G_0Q_0^2}{\alpha_0} + \frac{1}{2\Lambda_0}\left[1 - \left(1 - \frac{4G_0Q_0^2\Lambda_0}{\alpha_0}\right)^{3/2}\right]} \tag{2.12}$$

$$M_2 = \frac{1}{3G_0}\sqrt{\frac{6G_0Q_0^2}{\alpha_0} + \frac{1}{2\Lambda_0}\left[1 + \left(1 - \frac{4G_0Q_0^2\Lambda_0}{\alpha_0}\right)^{3/2}\right]}. \tag{2.13}$$

For the case of negative cosmolgical constant $\Lambda_0 < 0$, there is only one critical mass $\tilde{M} \equiv M_1$ for which the cosmological and the Schwarzschild horizon merge. For $M > \tilde{M}$ one finds two physical horizons at

$$\tilde{r}_1 \equiv r_1, \tag{2.14}$$

$$\tilde{r}_2 \equiv r_2 \quad , \tag{2.15}$$

whereas for $M < \tilde{M}$ the physical horizons disappear and one finds a naked singularity. This behavior is shown on the left hand side of figure 2.1. For the de Sitter case ($\Lambda_0 > 0$) a cosmological horizon appears, given by

$$r_c = \sqrt{\frac{3}{2\Lambda_0}} \left(1 + \sqrt{1 + \frac{4G_0 Q_0^2 \Lambda_0}{3\alpha_0}} \right)^{1/2} = r_4|_{M=0} \quad , \tag{2.16}$$

which for $Q_0 \to 0$ recovers the cosmological horizon of the Schwarzschild-de Sitter case. On the other hand, for $\Lambda_0 \to 0$ the cosmological horizon (2.16) vanishes and the horizons r_1 and r_2 turn out to be identical to the Reissner-Nordström case. Thus, the existence of an intermediate horizon r_2 in dS is limited to a maximal and a minimal mass parameter M as it can also be seen from figure 2.1b. Among those horizons, the external horizon (2.5) is of special interest, since it allows to calculate the Hawking temperature [4, 5] by

$$T = \frac{1}{4\pi} f'(r)|_{r=r_2} \quad . \tag{2.17}$$

Even though this concept of temperature has been derived for black hole actions that are solutions of the classical field equations, it will be also applied to the improved solutions, which have the same asymptotic behavior at infinity.

An other particularly interesting concept for charged black holes is the cosmic censorship hypothesis. This has two forms, the weak and strong censorship. The weak states that that in a process of gravitational collapse, the space-time singularities are hidden by event horizons. In other words, one expect only to find black holes that have horizons, such that the singularity is "dressed" by the horizon [7]. For the solutions presented here, cosmic censorship condition implies that only those black holes are physical that have at least one real valued inner horizon. This condition is solved by equation (2.12),

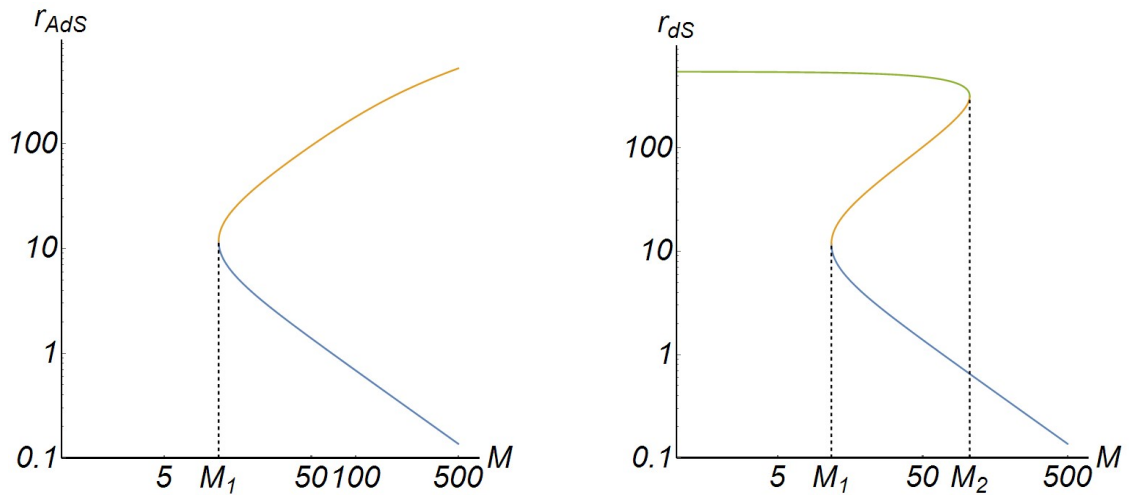

(a) (b)

FIG. 2.1. (a) Horizons for the AdS case as a function of the mass parameter M. The blue line corresponds to the inner horizon $\tilde{r}_1$ and the yellow line to the outer horizon $\tilde{r}_2$. The merging occurs at $M_1 \approx 11.7$. (b) Horizons for the dS case as a function of the mass parameter M. The blue line corresponds to the inner horizon r_1, the yellow line to the outer horizon r_2 and the green line to the cosmological horizon r_4. The outer and the inner horizons merge at mass values very close to the AdS case $M_1 \approx 11.7$. In addition to this the outer and the cosmological horizon merge at a mass parameter $M_2 \approx 105.6$. The remaining parameters were chosen as $G_0 = 1, Q_0 = 1, \alpha_0 = 1/137, \Lambda_0 = \pm 10^{-5}$.

which, for given parameters (Λ_0, Q_0 ...), implies a minimal physical mass. In figure 2.2 it is illustrated, how this minimal physical mass depends on the charge of a given (A)dS solution. One observes that for $\Lambda_0 \neq 0$, simple linear relation of the Reissner-Nordström censorship

$$M_{crit}|_{\Lambda_0=0} = Q_0/\sqrt{G_0\alpha_0} \quad , \tag{2.18}$$

gets modified for larger values of Q_0.

III. RENORMALIZATION GROUP FLOWS IN QUANTUM EINSTEIN GRAVITY COUPLED TO QED

In the Einstein-Hilbert truncation coupled to an electromagnetic sector, the effective action is given by [33, 34]

$$\begin{aligned}\Gamma_k &= \Gamma_k^{\text{grav}} + \Gamma_k^{\text{“QED”}} \\ &= \frac{1}{16\pi G_k}\int d^4x\sqrt{g}[-R + 2\Lambda_k] - \frac{1}{4\alpha_k}\int d^4x\sqrt{g}F_{\mu\nu}F^{\mu\nu} \quad ,\end{aligned} \tag{3.1}$$

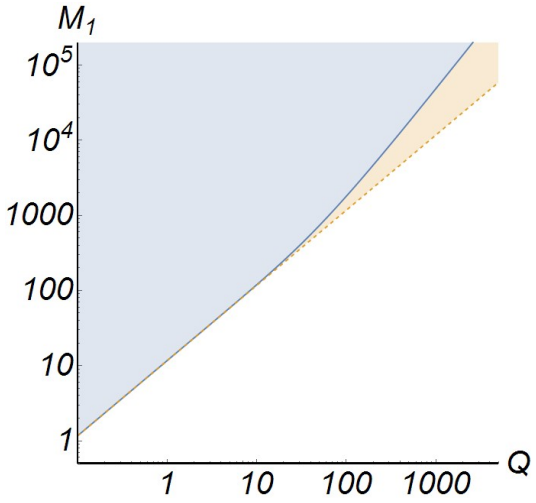

FIG. 2.2. Cosmic censorship scenario, where we plot the equation (2.12) in the AdS case. The blue line indicate the minimal mass values for the black hole has horizons and the blue zone represents the set of parameters that ensures weak cosmic censorship. The dashed orange line is the Reissner Nordström limit $Q_0/\sqrt{G_0\alpha_0}$. We use the values $\alpha_0 = 1/137$, $G_0 = 1$ and $\Lambda_0 = -10^{-5}$.

where the three coupling constants are, the Newton coupling G_k, the cosmological coupling Λ_k, and the electromagnetic coupling α_k (in terms of the fine structure "constant"). The scale dependence of those couplings is indicated by the subindex k which has energy dimension one. The dimensionless couplings are obtained from the dimensionfull couplings by multiplying with the corresponding power of k

$$g_k = G_k k^2, \qquad \lambda_k = \Lambda_k k^{-2}, \qquad \alpha_k = \alpha_k \quad . \tag{3.2}$$

The evolution of the dimensionless couplings (3.2) is governed by the renormalization group equations [14, 15, 34].

$$k\partial_k g_k = \beta_g(g_k, \lambda_k) \ , \qquad k\partial_k \lambda_k = \beta_\lambda(g_k, \lambda_k) \ , \qquad k\partial_k \alpha_k = \beta_\alpha(g_k, \alpha_k) \ . \tag{3.3}$$

The beta functions corresponding to g and λ are calculated in [14] and the beta function for α is obtained in [33] for the general case of Einstein-Hilbert action coupled to a Yang-Mills field and adaptated in [34] for the QEG picture coupled to QED. All these β-fuctions are computed in a d-dimensional spacetime, independent of the curvature of the gravitational background. For $d = 4$ one obtains

$$\beta_\lambda(g,\lambda) = (\eta_N - 2)\lambda + \frac{1}{2\pi} g \left[10\Phi_2^1(-2\lambda) - 8\Phi_2^1(0) - 5\tilde{\Phi}_2^1(0) \right], \tag{3.4}$$

$$\beta_g(g,\lambda) = (2 + \eta_N) g \ , \tag{3.5}$$

$$\beta_\alpha(g,\alpha) \equiv \left(A h_2(\alpha) - \frac{6}{\pi} \Phi_1^1(0) g \right) \alpha \quad . \tag{3.6}$$

The anomalous dimension of the gravitation coupling is given by

$$\eta_N(g,\lambda) = \frac{g B_1(\lambda)}{1 - g B_2(\lambda)} \quad , \tag{3.7}$$

where the two functions of the adimensional constant λ are given by

$$B_1(\lambda) \equiv \frac{1}{3\pi} \left[5\Phi_1^1(-2\lambda) - 18\Phi_2^2(-2\lambda) - 4\Phi_1^1(0) - 6\Phi_2^2(0) \right], \tag{3.8}$$

$$B_2(\lambda) \equiv -\frac{1}{6\pi} \left[5\tilde{\Phi}_1^1(-2\lambda) - 18\tilde{\Phi}_2^2(-2\lambda) \right] \quad . \tag{3.9}$$

The functions Φ_i have been calculated in the "optimised cutoff" sheme [35, 36]

$$\Phi_n^p(w) = \frac{1}{\Gamma(n+1)} \frac{1}{(1+w)^p} \ , \qquad \tilde{\Phi}_n^p(w) = \frac{1}{\Gamma(n+2)} \frac{1}{(1+w)^p} \quad . \tag{3.10}$$

Finally, the constant A and the function $h_2(\alpha)$ in equation (3.6) are defined in [34].
The RG equations (3.3) can be solved numerically, and depicted as a three dimensional flow graphic 3.1. One observes, the existence of a non trivial fixed point at which $\beta_g = 0,\ \beta_\lambda = 0$ and $\beta_\alpha = 0$. This fixed point is located at the coupling values

$$g_* = 0.707 \ , \qquad \lambda_* = 0.193 \ , \qquad \alpha_* = 6.365 \tag{3.11}$$

and it is approached in the UV by specific set of trajectories. By using (3.11) the dimensionfull coupling constants can be approximated at the vicinity of this fixed point

$$\lim_{k\to\infty} G_k = g_* k^{-2}, \quad \lim_{k\to\infty} \Lambda_k = \lambda_* k^2, \quad \lim_{k\to\infty} \alpha_k = \alpha_* \quad . \tag{3.12}$$

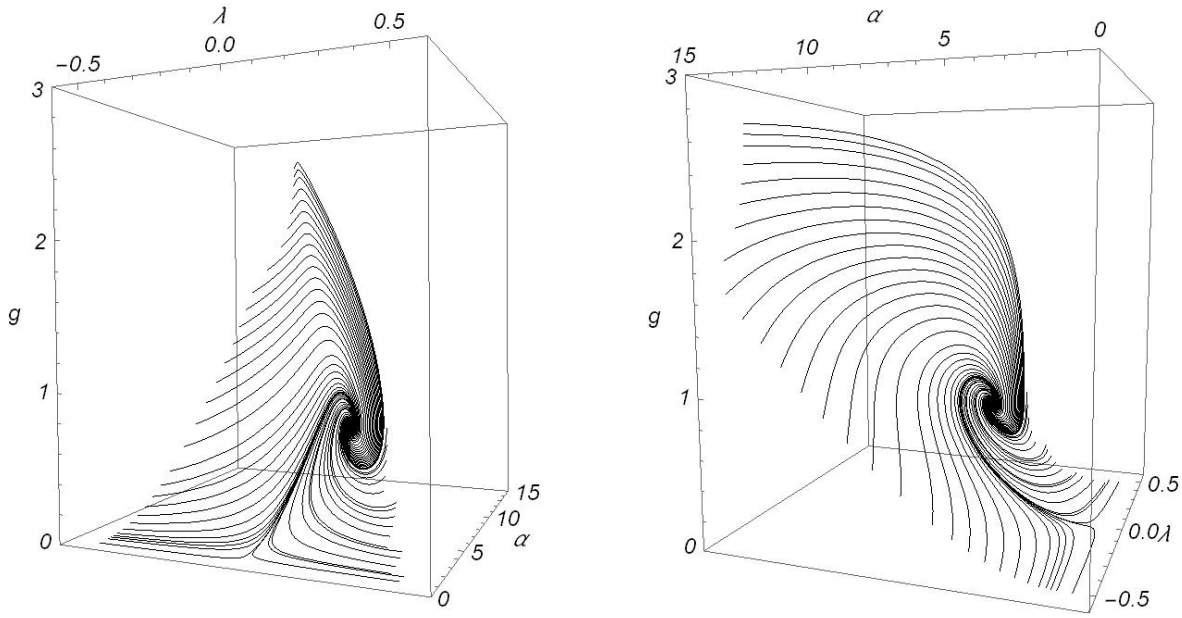

(a) (b)

FIG. 3.1. RG flow of the three couplings $g(k)$, $\lambda(k)$, and $\alpha(k)$ that solutions of (3.3) with the non-trivial fixed point (3.11).

It is sometimes convenient to work with analytic approximations of the renomalization group flow (3.3) in this case the following approximation will be used [29, 34, 37, 38]

$$g(k) = \frac{G_0 k^2}{1 + \frac{G_0}{g_*}(k^2 - k_0^2)}\,, \tag{3.13}$$

$$\lambda(k) = \frac{\Lambda_0}{k^2} + \lambda_* \left(1 - \frac{k_0^2}{k^2}\right) + \frac{g_* \lambda_*}{G_0 k^2} \log\left(\frac{1 + \frac{G_0}{g_*} k_0^2}{1 + \frac{G_0}{g_*} k^2}\right), \tag{3.14}$$

$$\begin{aligned}\alpha(k)^{-1} = &\left[1 + \frac{G_0}{g_*}(k^2 - k_0^2)\right]^{\frac{3\Phi g_*}{\pi}} \left[\frac{1}{\alpha_0} - \frac{g_*}{\alpha_* G_0 k_0^2}\ {}_2F_1\left(1, 1, 1 + \frac{3\Phi g_*}{\pi}; 1 - \frac{g_*}{G_0 k_0^2}\right)\right] \\ &+ \frac{g_*}{\alpha_* G_0 k^2}\left[1 + \frac{G_0}{g_*}(k^2 - k_0^2)\right]\ {}_2F_1\left(1, 1, 1 + \frac{3\Phi g_*}{\pi}; \frac{G_0 k_0^2 - g_*}{G_0 k^2}\right) \quad ,\end{aligned} \tag{3.15}$$

where ${}_2F_1$ is the hypergeometric function and $\Phi \equiv \Phi_1^1(0) = 1$ is evaluated using (3.10). Apart from the closed analytic form those approximated functions have the advantage that they have a well defined infra-red limit $k \to k_0$ as it can be seen from taking the limit with

$$g(k) \to G_0 k_0^2,\ \lambda(k) \to \Lambda_0 / k_0^2,\ \alpha(k) \to \alpha_0 \quad .$$

IV. SCALE SETTING FOR CLASSICAL BACKGROUNDS

Due to the renormalization program the coupling constants become scale dependent quantities. In the context of the Einstein -Hilbert - Maxwell action (3.1), this means

$$G \to G_k,\ \Lambda \to \Lambda_k \text{ and } \alpha \to \alpha_k \quad , \tag{4.1}$$

where k is an arbitrary scale of mass dimension one. If one is interested in a particular physical context, one tries to set the arbitrary scale in terms of characteristic physical quantities of the system under consideration. This step is crucial for the physical interpretation of the running couplings, in particular in extreme situations, where the scale dependence can become strong [22, 23, 27–29, 39–48] . Throughout this paper we will follow the procedure outlined in [22, 23] which relates the arbitrary energy scale to an inverse distance scale $k \propto 1/d$. This type of approach is well motivated since in the context of QED it allows to obtain the well known and well tested Uehling potential [21]. It is interesting to note that the electromagnetic coupling used in this paper (3.15) can be written like the usual running coupling of QED $\alpha^{-1}(k) = -A\ln(k) + c$, where $c = -A\gamma\psi(3\Phi g_*/\pi)$, γ is the Euler constant, and ψ is the Digamma function [34]. For spherically symmetric black holes with mass and charge in a cosmological background, the physical quantities characterizing the system are $\alpha_0, Q_0, G_0, M_0,$ and Λ_0, which will be assumed to be determined at some large radial scale r_0. In additional to those quantities there is the radial parameter r, which is expected to play a crucial role in the scale dependence. Thus, the scales k and d from the relation $k \propto 1/d$ will be functions of those physical quantities defined at large distance

$$k(r, \alpha_0, Q_0, G_0, M_0, \Lambda_0) = k(r) \equiv \frac{\xi}{d(P(r), \alpha_0, Q_0, G_0, M_0, \Lambda_0)} \quad , \tag{4.2}$$

where $P(r)$ is the point in space-time that one likes to study and $d(P)$ is a characteristic length scale separating this point from the black hole. Please note that using the relation (4.2) one assumes implicitly that the black hole is imbedded in vacuum. For example, if the black hole would be surrounded by some non-negligible matter density $\rho(r)$ this would introduce a new local energy scale which could replace (4.2) as the dominant infrared cutoff. The dimensionless parameter ξ in (4.2) controls the importance of scale

dependence, in the sense that zero or small ξ corresponds to zero or weak scale dependence. Here, $d(r)$ will be identified with the absolute proper radial distance between the center of the black hole and the point P calculated along a radial curve $\mathcal{C}_r$ [23]

$$d(P(r)) = \int_{\mathcal{C}_r} \sqrt{|ds^2|} \quad . \tag{4.3}$$

Please note that different choices for this length scale give typically very similar results [27, 28]. For the black hole metric (2.1), this length scale reads

$$d(r) = \int_0^r \frac{dr}{\sqrt{|f(r)|}} = \int_0^r \frac{dr}{\sqrt{|1 - \frac{2G_0M_0}{r} + \frac{G_0Q_0^2}{\alpha_0 r^2} - \frac{1}{3}\Lambda_0 r^2|}} \quad . \tag{4.4}$$

In figure 4.1, the radial dependence of $k/\xi = 1/d(r)$ is shown in the dS and the AdS case, for various different masses. One observes that the $k(r)$ is monotonically decreasing, with its steepest dependence on the horizons of the classical line element. The dS scale presents three visible vertical steps, one at the internal black hole horizon (which comes due to the charge contribution to the metric), one at the outer horizon, and another one at the cosmological horizon, the latter is absent in the AdS case. Another important point is that the biggest step (yellow line) is for the extreme black hole, where the inner and outer horizons merge. The same holds for the dS case, where external and cosmological horizons merge (red line). The $\Lambda_0 = 0$ case is equivalent to the AdS case, because this two have the same horizon structure.

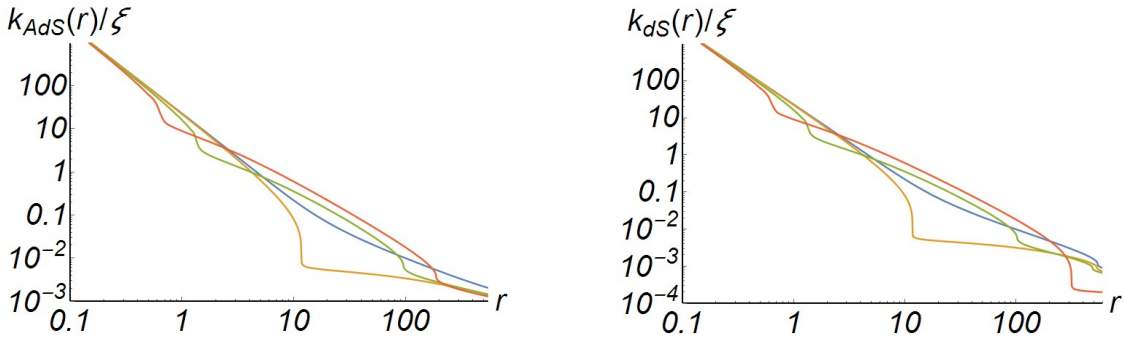

(a) (b)

FIG. 4.1. Dependence of the scale $k(r)/\xi$ according to (4.2) for $G_0 = 1, Q_0 = 1, \alpha_0 = 1/137, \Lambda_0 = \pm 10^{-5}$.
(a) AdS line element with masses M_0={5, 11.7, 50, 105.6} (blue, yellow, green, and red).
(b) dS line element with the same masses and color codings.

If one consider the pure Reissner-Nordström solution, we can compute an analytical solution for the proper distance, setting $\Lambda_0 = 0$ in (2.2) or (4.4), which is given by

$$d_{\rm RN}(r) = r\sqrt{f_{\rm RN}(r)} + G_0 M \log\left|r\sqrt{f_{\rm RN}(r)} + r - G_0 M\right| \\ + G_0 M \log\left|Q\sqrt{\frac{G_0}{\alpha_0}}\left(1 - \frac{M}{Q_0}\sqrt{\alpha_0 G_0}\right)\right| - Q\sqrt{\frac{G_0}{\alpha_0}} \quad , \tag{4.5}$$

where we defines $f_{\rm RN}(r) = f(r)|_{\Lambda_0=0}$. This solution only applies for masses different from the critical mass (2.18).

V. IMPROVED BLACK HOLE SOLUTION IN THE IR AND GLOBAL BEHAVIOR

In one way or the other, the scale dependence of the couplings ($G_k,\ \Lambda_k,\ \alpha_k$) in the effective action and the radial dependence of the actual scale setting $k(r)$, will have to result in a modification of the actual line element of the quantum corrected black hole space-time. As first approximation, which is expected to be most reliable in the IR, one can apply the "improving the classical solution" scheme [23, 49] , which implements the scale dependence based on correction of the classical line element (2.2).

1. Improved line element

In this improvement scheme one promotes the scale independent couplings, that are present in the classical solution, to the scale dependent quantities known from the RG flow (3.4)-(3.6)

$$f_k(r) = 1 - \frac{2g(k)M_0}{k^2 r} + \frac{g(k)Q_0^2}{\alpha(k)k^2 r^2} - \frac{1}{3}\lambda(k)k^2 r^2 \quad . \tag{5.1}$$

The arbitrary scale k becomes a physically relevant quantity due to the scale setting (4.2) shown in figure 4.1. With this scale setting one obtains the RG-improved metric function $f(r)$ shown in figure 5.1. For comparison, the purely classical solution is depicted in dashed lines and the solid lines are the RG-improved $f(r)$. Different curves correspond to different parameter choices. The ξ parameter in (4.2) is chosen, using a "self-consistent"

choice as in [27], (see also section V.2)

$$\xi_{sc}^2 \equiv \frac{3}{4\lambda_*} \quad , \tag{5.2}$$

In figure 5.1(a,b) one sees that the improved and the classical line elements are very similar for $r \gg M$, which is of course expected if given that the initial conditions for Λ_0, G_0, M_0, α_0, were obtained experimentally at the large r limit. On the other hand, in the (A)dS cases, in $r \ll M$ regime, the asymptotic behavior $r \to 0$ of the line element switches, which results in the appearance of a new internal horizon. From figure 5.1(c) one observes that only for $\Lambda_0 = 0$, the asymptotic behavior $r \to 0$ of the classical and the improved line element has the same sign and therefore no new horizon appears.

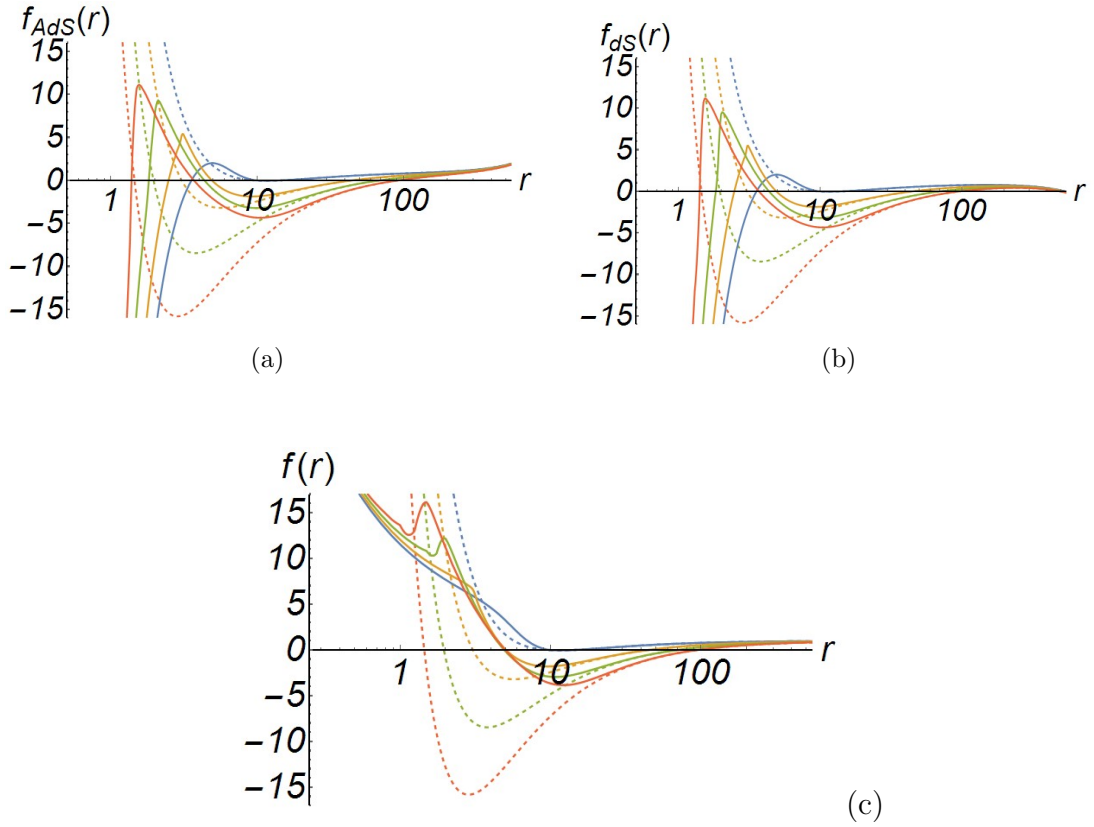

FIG. 5.1. Improved metric function for the self-consistent value ξ_{sc} for:
(a) AdS,
(b) dS, and
(c) Λ_0=0, with mass values M_0={12, 24, 36, 48} (blue, yellow, green, red), and $G_0 = 1, Q_0 = 1, \alpha_0 = 1/137, \Lambda_0 = \pm 10^{-5}$, $k_0 = 0.01$. The dashed lines are the classical metric function for each case, plotted for comparison.

One observes that in all three scenarios in figure 5.1(a,b,c), the outer black hole horizon

is slightly shifted towards smaller values as with respect to the purely classical solution.

One can further investigate the dependence of the improved functions for different ξ values. From figure 5.2 it can be seen that for larger ξ the difference between the improved and the classical solution is more pronounced and occurs at larger radial values, where the improvement have a single horizon. After this general study of the improved line

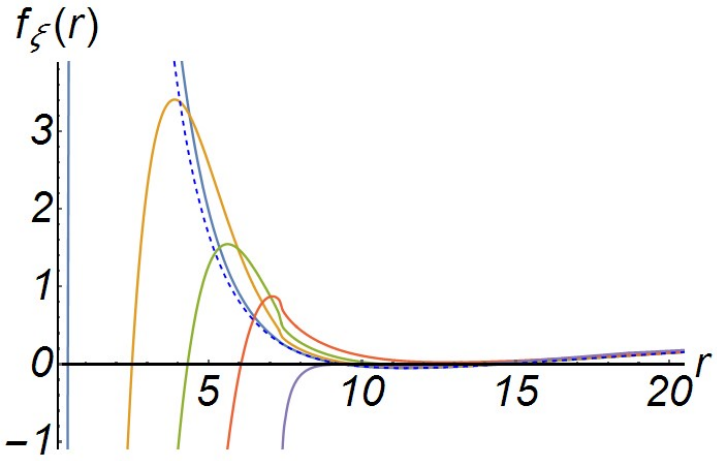

FIG. 5.2. Improved $f(r)$ for AdS case, setting the mass parameter $M_0 = 12$ and $G_0 = 1, Q_0 = 1, \alpha_0 = 1/137, k_0 = 0.01$. We use different ξ values, $\xi = \{0.5,\ 1.5,\ 2.5,\ 4,\ 11\}$ (blue, yellow, green, red, purple) and the dashed line correspond to the classical solution for comparison with the same parameters. There is a good agreement of the RG-improvement and the classical solution in the limit $\xi \ll 1$.

element, one can now turn to more specific physical aspects such as horizon structure, cosmic censorship, and temperature.

2. Alternative improvement schemes and improving the improved

There is no rigid principle imposing the scale setting prescription. Still, as long as one chooses a physically reasonable quantity for the renormalization scale k one can expect that the "improving solutions scheme" gives a better description of the system under consideration. This works for example for the Uehling potential [21]. In the case of improved black hole solution an alternative choice for the renormalization scale k would be for example in terms of the proper time rather than in terms of the proper distance. The length scale associated to the proper time is

$$k(r) = \frac{\xi}{\tau(r)} = \xi \left(\int_0^r dr' \left(f(r) - f(r') \right)^{-1/2} \right)^{-1} \quad . \tag{5.3}$$

One can compute this scale numerically and compare it with the corresponding proper distance, numerical or analytical (4.5). For the Reissner Nordstrom case this is done in figure 5.3. One observes that the choice of the scale setting has no important effect on the form of the improved metric.

$$\tau_{RN}(r) = \int_0^r dr' \left(\frac{2G_0 M}{r'} - \frac{G_0 Q^2}{\alpha_0 r'^2} - \frac{2G_0 M}{r} + \frac{G_0 Q^2}{\alpha_0 r^2} \right)^{-1/2} \quad . \tag{5.4}$$

In order to see to which extend such a different choice would affect the results of the

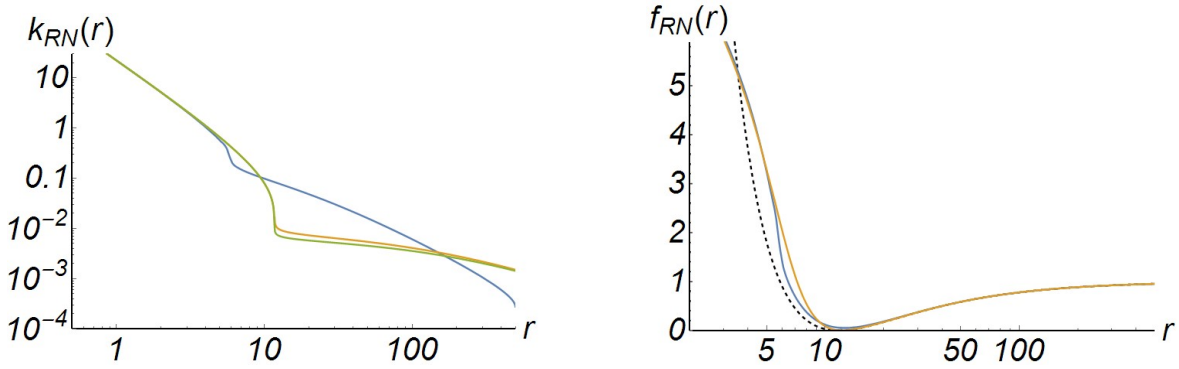

(a) (b)

FIG. 5.3. (a) Comparison of the proper time (blue) and numerical distance (orange) and analytical distance (green) scale settings, using $G_0 = 1, Q_0 = 1, \alpha_0 = 1/137$ and a mass value $M \simeq M_{crit}|_{\Lambda_0=0}$ (The analytical calculation is plotted only to compare with the numerical integration). One can see that both settings are basically the same until $r \sim 5$. Above that, one can see differences between the curves. (b) $f(r)$ improved functions for the two scales settings. We use the same values for the constants and ξ_{sc}. One can see not much differences between the 2 scale settings at a improved solution level.

previous section in the AdS case we show in figure 5.4(a) the radial dependence of the $k(r)$. One sees that difference between both scale settings are rather moderate. In figure 5.4(b) it is further shown how this difference reflects in the improved metric function. Luckily, one can see that no qualitative changes appear and that quantitative changes are moderate. Such, an insensitivity to different scale settings is something which is desirable.

When doing such improvements one would hope that the improvement gets one as close to the actual answer as possible. One encouraging finding in this sense would be for example that iterating the improvement procedure converges to a stable line element. Which choice for ξ in (4.2) is optimal in this sense? In order to get an analytic expression

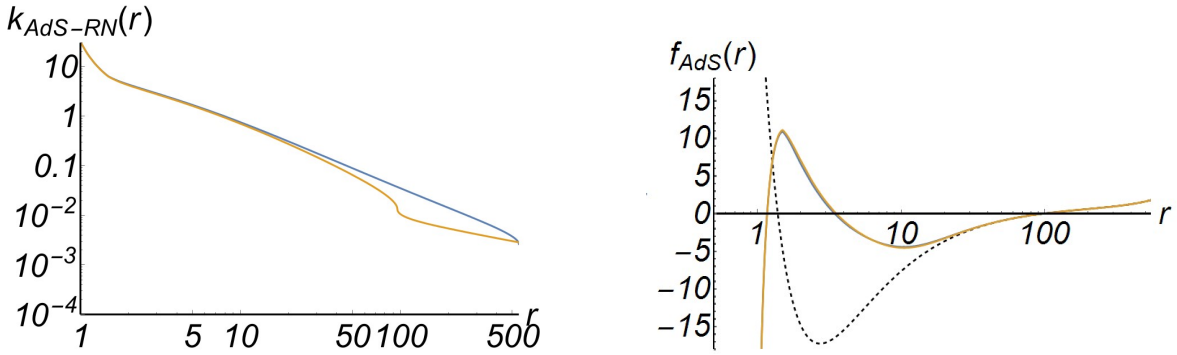

(a) (b)

FIG. 5.4. (a) Comparison of the proper time (blue) and distance (orange) scale setting. (b) Comparison of the improved metric function (5.1) using proper time (blue) and proper distance (orange). Also we plot the classical solution, in black dashed, for reference. For both plots we are using ξ_{sc} and $G_0 = 1, Q_0 = 1, \alpha_0 = 1/137, \Lambda_0 = -10^{-5}$, $k_0 = 0.01$ and $M = 50$. For the de Sitter case, there is no difference between scale settings and so with the improved functions.

for ξ, one can calculate (4.4) in the high energy limit ($r \ll 1$)

$$d(r) \simeq \frac{1}{2}\sqrt{\frac{\alpha_0}{G_0 Q_0^2}} r^2 \left[1 + \frac{2}{3}\frac{M_0 \alpha_0^2}{Q_0^2} r + \mathcal{O}(r^2)\right]. \tag{5.5}$$

(this procedure is shown in detail in Appendix). Once this is done, one can get $f(r)$ in UV limit, which is defined as $f_*(r)$ (7.4). With this new function, one can calculate a new $d(r)$, given by

$$d_*(r) \simeq \frac{\sqrt{3}}{4}\frac{1}{Q_0 \xi}\sqrt{\frac{\alpha_0}{G_0 \lambda_*}} r^2. \tag{5.6}$$

Comparing the first order improvement (5.5) and the second order improvement (5.6), one finds that both length scales agree, indicating a (UV) convergence of the improvements if one chooses

$$\xi^2 = \xi_{sc}^2 \equiv \frac{3}{4\lambda_*} \quad . \tag{5.7}$$

This UV-stable choice is similar to the choice which was in previous studies called "self consistent" [27, 28].

The framework of modern quantum field theory offers tools to study specific physical systems that go beyond the "improving solutions" approach. In principle one can for example derive the quantum "effective action". The equations of motion for this effective action are known as "gap equations" and they are typically non-local higher order differential equations, which are very difficult to solve. Still, when restricting to the lead-

ing local operators, those equations reduce to second order equations [50]. By assuming spherical symmetry and that the matter part of the stress energy tensor vanishes exactly for all $r \neq 0$, one can sometimes solve those gap equations with a Schwarzschild ansatz $g_{00} = -1/g_{11} \equiv \tilde{f}(r)$. Such solutions have been found for the Einstein-Maxwell system and for the Einstein-Hilbert system [47]. It is interesting to compare the behavior of the metric functions obtained from the improving solutions approach $f_{imp}(r)$ and the metric function that solves exactly the simplified version of the gap equations $\tilde{f}(r)$. One finds that both quantum improved descriptions have a well defined classical limit

$$\begin{aligned} \lim_{\xi \to 0} f_{imp}(r) &= f_{cl}(r), \\ \lim_{\epsilon \to 0} \tilde{f}(r) &= f_{cl}(r). \end{aligned} \tag{5.8}$$

A comparison of both functions is shown in figure 5.5 for

$$\tilde{f}(r) = \frac{r^4\epsilon^2\alpha_0 + 4\epsilon r^3\alpha_0 + 4(1 - G_0 M_0 \epsilon) r^2 \alpha_0 - 8 r G_0 M_0 \alpha_0 + 4 G_0 Q_0^2}{4 r^2 (\epsilon r + 1)^2 \alpha_0} \tag{5.9}$$

One observes that $f_{imp}(r)$ produces short distance corrections to the classical function $f_{cl}(r)$, while $\tilde{f}(r)$ produces large distance corrections to $f_{cl}(r)$. Since one expects quantum corrections to be relevant rather at short distance scales than at large distance scales, one can conclude that at this level the "improving solutions" approach meets much better our physical expectations than the "solving improved actions" approach. This seems to indicate that the short distance corrections of improved actions come from higher order, or even non-local operators. This raises very interesting questions and possibilities for future investigations, in particular when working with a "solving improved actions" approach.

3. Modified horizon structure, cosmic censorship, and temperature

As discussed above, the RG-improvement induces for $\Lambda_0 \neq 0$ a structural change in the horizon structure of the black hole. The most important feature is that a new internal horizon appears due to the improvement. It is interesting to note that this new horizon exists even for masses below the critical mass value M_1. Since, one expects (and observes) that the improved solutions turns into the classical solution for $\xi \to 0$ one has to understand how such a drastic feature, as the appearance of a new internal horizon,

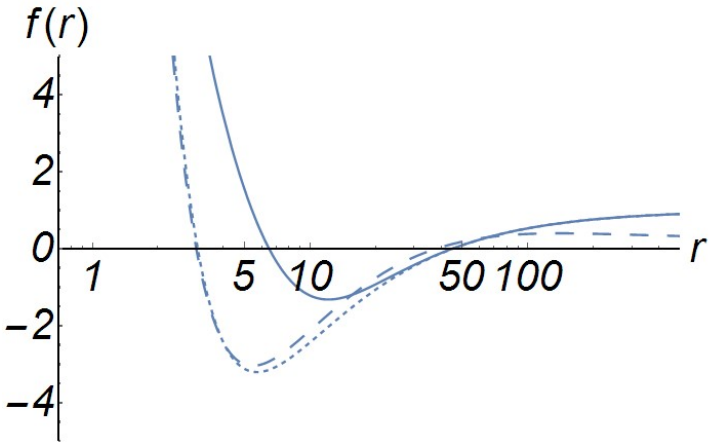

FIG. 5.5. Comparison of $\tilde{f}(r)$ (dashed), $f_{imp}(r)$ (line) and $f_{cl}(r)$ (point) for the Reissner-Nordstöm black hole, using ξ_{sc}, $\epsilon = 0.01$, $G_0 = 1, Q_0 = 1, \alpha_0 = 1/137, \Lambda_0 = -10^{-5}$, $k_0 = 0.01$ and $M = 15$

fits into this picture. In order to understand this, one can plot the improved horizon structure as a function of the black hole mass, just as it was done in the classical figure 2.1. By varying the ξ parameter in figure 5.6 one understands how the improved horizon structure, with its additional horizon, fits to the classical horizon structure. Due to the improvement, the classical inner horizon (dashed line) is split into two horizons, one with larger radius and the other one with smaller radius than the classical inner horizon. For smaller and smaller values of ξ the larger one of the internal horizons aligns with the classical inner horizon, whereas the smaller additional horizon radius gets shifted towards $r_{(A)dS} \to 0$ recovering the classical behavior. Still, as long as $\xi \neq 0$, this new inner horizon persists, even for masses below M_1. The fact that there is a horizon below the critical mass is important for cosmic censorship hypothesis. In figure 2.2, it was noted that there is a critical mass M_c below which a naked singularity can appear. From figure 5.6 one sees that this critical mass is pretty much unaffected by the improvement procedure. However, the existence of a new internal horizon protects the improved black hole against the appearance of a naked singularity, even for a arbitrarily small mass parameter M_0. This means that, (for this choice of parameters –scale setting), the weak cosmic censorship is fulfilled.

One of the most exciting facts about black holes is that they have a thermodynamic behavior, which leads to a (quantum driven) evaporation process. For describing this evaporation process for the classical black hole solution on uses the relation (2.17), which can be obtained from a comparison of the boundaries of this solution with the asymp-

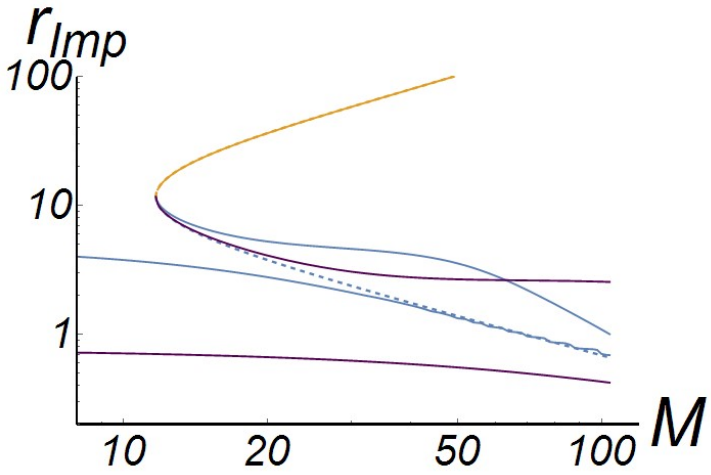

FIG. 5.6. Improved Horizons, for dS black holes. The orange line corresponds to the external horizon and the blue lines are for internal horizons. Also we have purple lines, that correspond to internal horizons for $\xi = \xi_{sc}/3$. The dotted line is for the classical horizon. The values used are $G_0 = 1, Q_0 = 1, \alpha_0 = 1/137, k_0 = 0.01$, and ξ_{sc}. For AdS black holes we have the same behavior.

totic behavior of empty space-time. However, the space-time of the improved black hole solution has the same asymptotic behavior as the classical solution for large r. Therefore, changes of the thermodynamic behavior due to the improved line element must be also encoded at the black hole horizon and not in the large r asymptotics. Therefore, it reasonable to use the relation (2.17) for the description of the evaporation process of the improved black hole, where the relation has then to be evaluated at the outer-inner horizon [4, 5]. In figure 5.7 the temperature of the improved black hole space-time is shown in dashed lines as a function of the mass parameter M_0 in comparison to the classical temperature. The three different colors correspond to the dS, the AdS and the $\Lambda_0 = 0$ case. One observes that the improvement tends to lower the temperature of the improved black hole with respect to the classical black hole independent of Λ_0. This difference in temperature is relatively small for the entire mass range. Still one observes that it vanishes for large masses and is most pronounced for smaller masses. Notably, the critical mass at which the temperature changes drastically is the same for the classical and the improved case. This, can already be understood with figure 5.6, since it is the mass at which two of the horizons merge, which occurs to the same for the improved and the standard case. However, while the temperature in the standard case drops to zero at this critical mass, the improved solution provides a phase transition due to the additional

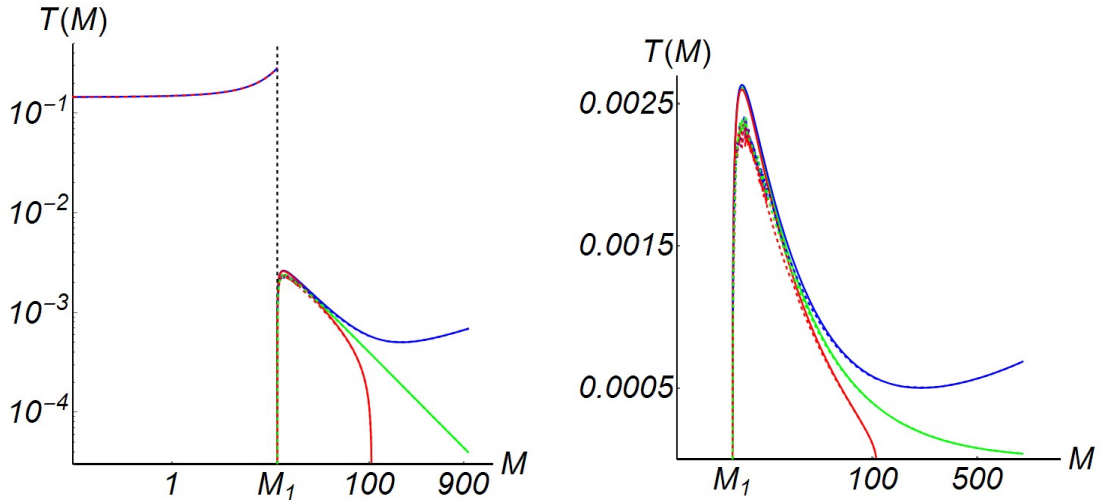

(a) (b)

FIG. 5.7. Improved temperature as function of the mass parameter, evaluated in the external horizon for AdS (blue), dS (red) and $\Lambda_0 = 0$ (green) cases. Also, we plot in full lines the classical temperature (2.17) evaluated in r_2 (2.5). The values chosen for evaluation are $G_0 = 1, Q_0 = 1, \alpha_0 = 1/137, k_0 = 0.01$: (a) shows the behavior for a large range of masses, where for $M < M_1$ the improve temperature is evaluated in the new internal improved horizon.
(b) is a zoom for masses $M > M_1$.

inner horizon which becomes visible at masses $M < M_{crit}$. One observes that compared to this transition, modification from the non-improved temperature are rather mild.

4. Modified mass, charge

It is instructive to study how one would interpret the improved black hole solution is one would not be aware of a possible scale dependence of the couplings. In this case one would perform experiments at some radial scale r and assuming constant couplings G_0, Λ_0, and α_0. The result of such an experiment (say the study of sections of geodesics) would then be fitted by the "charges" of the black hole. For astrophysical distances, those charges would be basically the mass $M = M(r)$ and the electrical charge $Q^2 = Q^2(r)$, whereas the cosmological term with its corresponding "charge" $L = L(r)$ is largely irrelevant at a range of smaller radii. Taking equation (5.1) and redefining mass and charge in this sense of fitting the metric function one would write

$$f_k(r) = 1 - \frac{2G_0M(r)}{r} + \frac{G_0Q^2(r)}{\alpha_0 r^2} - \frac{1}{3}\Lambda_0 L(r) r^2 \quad , \tag{5.10}$$

with

$$M(r) \equiv \frac{M_0 g(k)}{G_0 k^2(r)} \quad , \tag{5.11}$$

and

$$Q(r) \equiv \frac{Q_0^2 \alpha_0}{G_0} \frac{g(k)}{\alpha(k) k^2(r)} \quad . \tag{5.12}$$

This analysis allows to get a feeling on how such renormalization group effects would appear to an unprepared observer. Figure 5.8 shows the radial dependence of the effective mass (5.11) and the effective charge (5.12). One observes that for large radii, the effective

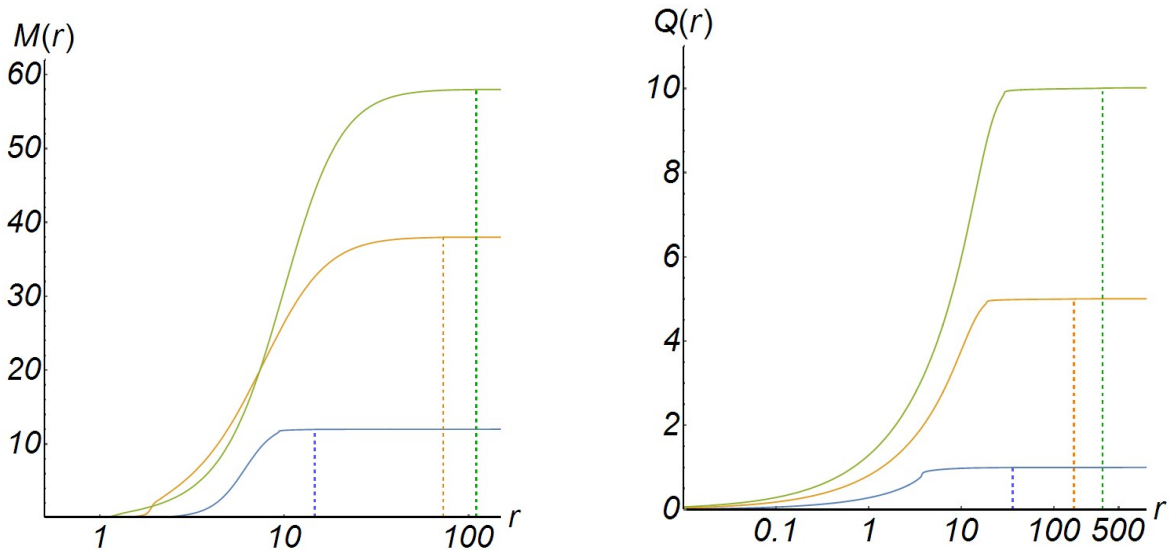

(a) (b)

FIG. 5.8. Mass and charge as variables dependent of r for AdS case:
(a) The different curves are for the mass values $M_0 = \{12,\ 38,\ 58\}$ (from bottom to top), and fixed charge $Q_0 = 1$.
(b) The curves are for the charge values $Q_0 = \{1,\ 5,\ 10\}$ (from bottom to top) with mass values $M_0 = \{20,\ 100,\ 250\}$, respectively. The other parameters $\xi_{sc},\ G_0 = 1,\ \alpha_0 = 1/137,\ k_0 = 0.01$. The dS case is basically identical since differences only would occur at extremely large radii.

masses and charges are basically identical to the value of the classical parameters M_0 and Q_0. However, for smaller radii, the effective mass and effective charge of the improved black hole are driven to smaller and smaller values, reflecting a screening effect of the scale dependence, that becomes effective for large scale k and small scales r.

VI. CONCLUSIONS

This paper studied the effects of renormalization group induced scale dependence on the charged dS and AdS black hole solutions. This is done by applying the "improving classical solutions" method suggested by Bonnano and Reuter [23]. After introducing the scale dependent couplings in the classical solution (5.1), the arbitrary scale k is set to physically relevant quantity by (4.2) resulting in the line element of the improved black hole. This line element shows agreement with the classical line element for large radial coordinates and increasing deviations for small radial coordinates. The relative amount of corrections due to the renormalization group effects is controlled by the ξ parameter, defined in (4.2). This parameter is implemented such that $\xi \to 0$ recovers the classical solution, while increasing ξ implies increasing relevance of the renormalization group effects. As the name indicates, the improved black hole space-time is to be understood as first short distance correction with respect to the classical result. In this spirit the short distance improvement is formulated as an iterative process, where an improved line element is used as bases for repeating the improvement process. The crucial question then is, whether this procedure converges or not. It is found that there exists a preferred choice for the parameter $\xi = \xi_{sc}$, which allows to get fastest "convergence" of the iterative procedure. This choice agrees with the "self-similar" choice proposed in [27] and it will be used as benchmark for the numerical studies.

The significance and meaning of the differences between improved and classical line elements and their dependence on the parameters is subsequently studied from various perspectives:

- Horizon structure: It turns out that the improved solutions have an additional internal horizon, which is present independent of the value of M_0

- Cosmic censorship: Classical charged black holes in (A)dS space have to invoke the cosmic censorship in order to avoid the appearance of a naked singularity at $r \to 0$. The improved charged black holes however, can count on an additional internal horizon, which protects against the appearance of this naked singularity.

- Temperature: Like in the uncharged case [27], the evaporation of the improved black hole does not stop at some remnant mass. But the improved charged black holes

have the additional feature that at a mass corresponding to the classical critical mass M_{crit}, the black hole experiences a zero order transition in the temperature.

- Effective mass and charge: If one would not be aware of the scale dependence of the couplings one would associate changes in the line element to changes in the charges, in particular $M = M(r)$ and $Q = Q(r)$. One finds that those effective charges converge to the classical parameter M_0 and Q_0 at large radial parameters. However, at small radial parameters, the black hole appears to loose mass and charge, by virtue of the renormalization group improvement. Such an effect can have interesting observational consequences [51].

The result on the cosmic censorship is quite remarkable and closely related to the asymptotic behavior of the improved line element at small r. In order to understand this limit, the appendix A studies this effect analytically confirming the numerical observation of inverted asymptotics.

The work of B.K. was supported by Fondecyt 1120360 and Anillo Atlas Andino 10201. The work of C.G. was supported by Conicyt 21130928, Conicyt 81140256 and proy. Fondecyt 1120360.

Appendix A: RG-Improved black hole solutions in the UV

An analytical expression for $k(r)$ not be obtained, unless for very extreme regimes, such as very small radial coordinates, where one might dare to make an expansion in r

$$d(r) \simeq \frac{1}{2}\sqrt{\frac{\alpha_0}{G_0 Q_0^2}} r^2 \left[1 + \frac{2}{3}\frac{M_0 \alpha_0^2}{Q_0^2} r + \mathcal{O}(r^2)\right]. \tag{7.1}$$

The cosmological constant Λ_0 does not appear in this expansion until order r^6. With this expression for $d(r)$, at first order in r, one can get an analytic result for $k(r)$ given by

$$k(r) \simeq 2Q_0 \sqrt{\frac{G_0}{\alpha_0}} r^{-2} \xi. \tag{7.2}$$

Taking the UV limit, $k \to \infty$, one must use (3.12) in (5.1) obtaining

$$f_*(r) = 1 - \frac{2g_*M_0}{k^2 r} + \frac{g_* Q_0^2}{\alpha_* k^2 r^2} - \frac{1}{3}(\lambda_* k^2) r^2. \tag{7.3}$$

Using the analytic expression for $k(r)$, one gets

$$f_*(r) = 1 - \frac{\alpha_0 g_* M_0}{2G_0 \xi^2 Q_0^2} r^3 + \frac{\alpha_0 g_*}{4\alpha_* G_0 \xi^2} r^2 - \frac{4G_0 \lambda_* \xi^2 Q_0^2}{3\alpha_0 r^2} \ . \tag{7.4}$$

and the "self-consistent" improved function

$$f_{*,sc}(r) = 1 - \frac{2\alpha_0 g_* \lambda_* M_0 r^3}{3\mathrm{G}_0 Q_0^2} + \frac{\alpha_0 g_* \lambda_* r^2}{3\alpha_* \mathrm{G}_0} - \frac{\mathrm{G}_0 Q_0^2}{\alpha_0 r^2} \ . \tag{7.5}$$

One can see that this improved UV solution is analytically different from the classical solution (2.2). This is the origin of the differences of the complete improved and the classical solution that one can see in figure (5.1(a),(b)), because we can see this differences in the $r < M$ regime. Also, the fact that this UV approximation does not depend on the value of Λ_0, indicates that only in small distances is where differences are found.
Finally, with this difference of the classical and RG-Improved line element, one expects that some other structural modifications of the solution appears. One can compute the square of the Riemman-tensor of the UV RG-Improved solution (7.5), obtaining

$$R_{\mu\nu\rho\sigma} R^{\mu\nu\rho\sigma} = \frac{8\alpha_0^2 g_*^2 \lambda_*^2}{3\alpha_*^2 G_0^2} + \frac{304\alpha_0^2 g_*^2 \lambda_*^2 M_0^2 r^2}{9G_0^2 Q_0^4} - \frac{160\alpha_0^2 g_*^2 \lambda_*^2 M_0 r}{9\alpha_* G_0^2 Q_0^2} + \frac{64 g_* \lambda_* M_0}{3r^3} + \frac{56 G_0^2 Q_0^4}{\alpha_0^2 r^8} \ . \tag{7.6}$$

where one can see that the spatial singularity at the origin $r = 0$ remains. This mean that RG-Improve process does not resolve the singular behavior of the classical solution in contrast of the calculations made for Reuter and Bonanno [22] for Schwarzschild black holes where they remove the spatial singularity at the origin with the RG-Improvement.

[1] A. Celotti, J. C. Miller, and D. W. Sciama, Class. Quant. Grav. **16**, A3 (1999), arXiv:astro-ph/9912186 [astro-ph].

[2] R. Narayan and J. E. McClintock, (2013), arXiv:1312.6698 [astro-ph.HE].

[3] S. W. Hawking and R. Penrose, Proc. Roy. Soc. Lond. **A314**, 529 (1970).

[4] S. Hawking, Communications in Mathematical Physics **43**, 199 (1975).

[5] G. W. Gibbons and S. W. Hawking, Phys. Rev. D **15**, 2738 (1977).

[6] R. Penrose, General Relativity and Gravitation **34**, 1141 (2002), originally published on Riv. Nuovo Cim. **1**, 252 (1969).

[7] R. Penrose, Annals of the New York Academy of Sciences **224**, 125 (1973).

[8] S. W. Hawking and W. Israel, *General Relativity, An Einstein centenary survey* (Univ. Pr., Cambridge, UK, 1979).

[9] R. Penrose, J. Astrophys. Astron. **20**, 233 (1999).

[10] R. M. Wald, in *In *Iyer, B.R. (ed.) et al.: Black holes, gravitational radiation and the universe* 69-85* (1997) arXiv:gr-qc/9710068 [gr-qc].

[11] P. R. Brady, I. G. Moss, and R. C. Myers, Phys. Rev. Lett. **80**, 3432 (1998), arXiv:gr-qc/9801032 [gr-qc].

[12] S. Hod, Phys. Rev. Lett. **100**, 121101 (2008), arXiv:0805.3873 [gr-qc].

[13] S. Weinberg, in *Conceptual foundations of quantum field theory. Proceedings, Symposium and Workshop, Boston, USA, March 1-3, 1996* (1996) arXiv:hep-th/9702027 [hep-th].

[14] M. Reuter, Phys.Rev. **D57**, 971 (1998), arXiv:hep-th/9605030 [hep-th].

[15] M. Reuter and F. Saueressig, Phys.Rev. **D65**, 065016 (2002), arXiv:hep-th/0110054 [hep-th].

[16] M. Niedermaier and M. Reuter, Living Reviews in Relativity **9** (2006), 10.12942/lrr-2006-5.

[17] M. Reuter and F. Saueressig, in *First Quantum Geometry and Quantum Gravity School Zakopane, Poland, March 23-April 3, 2007* (2007) arXiv:0708.1317 [hep-th].

[18] R. Percacci, (2007), arXiv:0709.3851 [hep-th].

[19] D. F. Litim, *Proceedings, Workshop on From quantum to emergent gravity: Theory and phenomenology (QG-Ph)*, (2008), [PoSQG-Ph,024(2007)], arXiv:0810.3675 [hep-th].

[20] M. Reuter and F. Saueressig, New J.Phys. **14**, 055022 (2012), arXiv:1202.2274 [hep-th].

[21] E. A. Uehling, Phys. Rev. **48**, 55 (1935).

[22] A. Bonanno and M. Reuter, Phys. Rev. **D60**, 084011 (1999), arXiv:gr-qc/9811026 [gr-qc].

[23] A. Bonanno and M. Reuter, Phys. Rev. **D62**, 043008 (2000), arXiv:hep-th/0002196 [hep-th].

[24] A. Bonanno and M. Reuter, Phys.Rev. **D73**, 083005 (2006), arXiv:hep-th/0602159 [hep-th].

[25] M. Reuter and E. Tuiran, "Quantum Gravity Effects in Rotating Black Holes," in *The Eleventh Marcel Grossmann Meeting* (2006) Chap. 473, pp. 2608–2610, arXiv:hep-th/0612037 [hep-th].

[26] M. Reuter and E. Tuiran, Phys.Rev. **D83**, 044041 (2011), arXiv:1009.3528 [hep-th].

[27] B. Koch and F. Saueressig, Class.Quant.Grav. **31**, 015006 (2014), arXiv:1306.1546 [hep-th].

[28] B. Koch and F. Saueressig, Int.J.Mod.Phys. **A29**, 1430011 (2014), arXiv:1401.4452 [hep-th].

[29] B. Koch and I. Ramirez, Class.Quant.Grav. **28**, 055008 (2011), arXiv:1010.2799 [gr-qc].

[30] K. Lake, Phys. Rev. D **19**, 421 (1979).

[31] F. Mellor and I. Moss, Phys. Rev. D **41**, 403 (1990).

[32] L. J. Romans, Nucl. Phys. **B383**, 395 (1992), arXiv:hep-th/9203018 [hep-th].

[33] J.-E. Daum, U. Harst, and M. Reuter, JHEP **1001**, 084 (2010), arXiv:0910.4938 [hep-th].

[34] U. Harst and M. Reuter, JHEP **1105**, 119 (2011), arXiv:1101.6007 [hep-th].

[35] D. F. Litim, Phys. Rev. **D64**, 105007 (2001), arXiv:hep-th/0103195 [hep-th].

[36] D. F. Litim, Phys. Rev. Lett. **92**, 201301 (2004), arXiv:hep-th/0312114 [hep-th].

[37] C. Contreras, B. Koch, and P. Rioseco, Class.Quant.Grav. **30**, 175009 (2013), arXiv:1303.3892 [astro-ph.CO].

[38] B. Koch, C. Contreras, P. Rioseco, and F. Saueressig, (2013), arXiv:1311.1121 [hep-th].

[39] A. Bonanno and S. Carloni, New J. Phys. **14**, 025008 (2012), arXiv:1112.4613 [gr-qc].

[40] A. V. Frolov and J.-Q. Guo, ArXiv e-prints (2011), arXiv:1101.4995 [astro-ph.CO].

[41] A. Bonanno and M. Reuter, Phys. Rev. **D65**, 043508 (2002), arXiv:hep-th/0106133 [hep-th].

[42] A. Bonanno, Phys. Rev. **D85**, 081503 (2012), arXiv:1203.1962 [hep-th].

[43] M. Hindmarsh and I. D. Saltas, Phys. Rev. **D86**, 064029 (2012), arXiv:1203.3957 [gr-qc].

[44] K. Falls and D. F. Litim, Phys.Rev. **D89**, 084002 (2014), arXiv:1212.1821 [gr-qc].

[45] E. J. Copeland, C. Rahmede, and I. D. Saltas, Phys. Rev. **D91**, 103530 (2015), arXiv:1311.0881 [gr-qc].

[46] B. Koch, P. Rioseco, and C. Contreras, Phys. Rev. **D91**, 025009 (2015), arXiv:1409.4443 [hep-th].

[47] B. Koch and P. Rioseco, Class. Quant. Grav. **33**, 035002 (2015), arXiv:1501.00904 [gr-qc].

[48] A. Bonanno and A. Platania, Phys. Lett. **B750**, 638 (2015), arXiv:1507.03375 [gr-qc].

[49] W. Dittrich and M. Reuter, Lect. Notes Phys. **220**, 1 (1985).

[50] M. Reuter and H. Weyer, Phys. Rev. **D69**, 104022 (2004), arXiv:hep-th/0311196 [hep-th].

[51] D. C. Rodrigues, B. Koch, O. F. Piattella, and I. L. Shapiro, *Proceedings, Cosmology and gravitation in the Southern Cone (CosmoSur II)*, AIP Conf. Proc. **1647**, 57 (2015).